Int. J. Electrochem. Sci., 14 **(2019)** 8243 – 8255, doi: 10.20964/2019.08.102

International Journal of ELECTROCHEMICAL SCIENCE
www.electrochemsci.org

Effect of Heat Treatment on the Corrosion Behavior of Welded 7075 T6 Aluminum Alloy Without Filler Material

V.A. Arizmendi-Salgado[1], S.A. Serna[1], A. Torres-Islas[2], R. Soto-Espitia[3], P. Althuzer[4], S. Mejia-Sintillo[1], J. Campos-Alvarez[4], J.G. Gonzalez-Rodriguez[1]*

[1] Universidad Autonoma del Estado de Morelos, CIICAp, Av. Universidad 1001, 62209-Cuernavaca, Mor., Mexico
[2] Universidad Autonoma del Estado de Morelos, FCQeI, Av. Universidad 1001, 62209-Cuernavaca, Mor., Mexico
[3] Universidad Michoacana de San Nicolás de Hidalgo, Fac. de Ingeniería Civil.
[4] Universidad Nacional Autonoma de Mexico, Instituto de Energias Renovables, Priv. Xochicalco s/n, Temixco, Mor., Mexico
[*]E-mail: ggonzalez@uaem.mx

Received: 8 April 2019 / *Accepted:* 12 June 2019 / *Published:* 30 June 2019

A study on the effect of heat treatment and welding condition on the corrosion behavior of 7075T6 Al alloy without material contribution has been investigated in 3.5% NaCl solution. Electrochemical techniques included potentiodynamic polarization curves, linear polarization resistance (LPR) and electrochemical impedance spectroscopy (EIS) measurements. Heat treatments included solubilized, retrogression and re-aging (rra), and T73. After that, specimens were welded by the Tungsten inert gas (TIG) method without filler. Corrosion tests showed that the corrosion rates were very similar for both the base metal and welding. However, for the base metal, the highest corrosion rate was exhibited for the solubilized condition, whereas for the welding it was for the T6 condition. All specimens were highly susceptible to localized type of corrosion where the second phases acted as cathodes and the surrounding matrix acted as active anodes.

Keywords: Al alloy, heat treatment, welding.

1. INTRODUCTION

Due to a combination of properties that make it a very useful and that it is a metallic material very abundant in the earth surface, Aluminum, is widely used at an industrial and domestic level. Among its main characteristics, we can cite its low density, high thermal and electrical conductivity and low melting point, including the fact that when alloyed, its mechanical properties are [1, 2]. One of the main

industries that use it are the automotive sector, absorbs more than 25% of the aluminum that is produced in the world, aerospace, aeronautics, electronics and other fields of application due to its lightness [3].

Steels can be replaced by Aluminum alloys in several applications especially where weight are one of the limitations. However, their application are limited in the industry due to their low strength. Therefore, the development of Al alloys with improved mechanical properties is the goal of undergoing new research works [4, 5].The use of aluminum in transport construction has increased, this is because it helps reduce weight and improve fuel efficiency. The structures used in the transport industry are subject to a large number of cyclic loads, during their service life, favoring the appearance of cracks [6].This raises a major problem on how to join aluminum pieces both efficiently and economically [7]. Aluminum alloy 7075 is widely used in the aerospace industry for the design and manufacture of parts, for this reason this material must be welded to join several parts and elements that make up a structure. Two types of welding procedures exists, being the first one that occurs at high temperatures and involves both chemical and metallurgical reaction between the molten aluminum alloy and the matrix; the second one, involving mechanical interaction, occurs at low temperatures [8,9]. The Tungsten inert gas welding process (TIG) is used when a good welding appearance and high quality is required. Due to the fact that in the aforementioned industry there is a high percentage in the failure of structural elements, the need arises to improve the mechanical properties of said material through the application of thermal treatments [10] which improve the resistance to corrosion.

When metals are exposed to their surrounding environment, corrosion takes place, which is defined as the chemical reaction, natural and spontaneous, of the metallic material with the surrounding medium, through which the material loses or alters its properties. From this point of view, the corrosion behavior is one of the most determining criteria in the selection of a certain material, which will work under extreme conditions and sometimes in the presence of highly aggressive environments [11, 12]. The direct costs of corrosion in industrial activities have a different impact on the economy of each country, given that their scientific and technological characteristics vary [11].The technological development at present imposes a continuous search of new materials that satisfy a compendium of properties.

Due to its excellent mechanical properties and to the development of an external oxide spontaneously formed when exposed to air, Al alloys have been widely studied from the corrosion point of view. For instance, in [12] the corrosion behavior of aluminum alloy 6061 were prepared using different welding techniques such as shielded metal arc welding (SMAW), friction stir welding (FSW) and gas tungsten arc welding (GTAW). They were evaluated in 3.5% NaCl solution and evaluated with electrochemical techniques like potentiodynamic polarization curves and electrochemical impedance spectroscopy (EIS). These techniques best corrosion resistance was obtained the GTAWB method, whereas the lowest corrosion resistance was achieved by using the SMAW welding procedure. Similarly, in [13] corrosion tests in 3.5 % NACl solution were carried out with 7A52 Al alloy plates with the ER 5356 filler welded by the Twin-wire metal inert gas arc welding technique (TMW). The fusion and heat affected zones turned out to be the most corrosion susceptible places then the base metal. Thus, the present research work has been developed with the purpose of studying the corrosion behavior of AA 7075 aluminum alloy welded by TIG (without material contribution) at 200 A, under different aging conditions. This corrosive behavior was evaluated by means of electrochemical techniques using a 3.5%

NaCl solution. The obtained results in a previous work [14] showed that the $ZnMg_2$ and Al are the elements responsible for the η phases (along the grain boundaries) and η' (inside the grains); since they provide a resistance to corrosion without sacrificing the mechanical properties of the alloy, this is due to the thermal treatment of retrogression and re-aging.

2. EXPERIMENTAL PROCEDURE

2.1 testing material

Table 1. Chemical composition of 7075-T6 aluminum alloy (wt. %).

7075 T6	Al	Zn	Cu	Mg	Mn
	Base	5.1 – 6.1	1.2 – 2.0	2.1 – 2.9	0.3

Material used in this research work includes plates 6 mm thick by 500 mm long and 70 mm wide of 7075-T6 aluminum alloy with a chemical composition as given in table 1. The welded samples were cut into dimensions of 1.0 cm^2 of exposure area to apply the following heat treatments:

i) Solubilization, at a temperature of 470 °C for one hour, which serves as a platform to perform the subsequent aging, where the $MgZn_2$ precipitates present in the alloy are dissolved [15].

ii) T73, consists of raising the temperature up to 470 ºC during one hour, then cool it down to 120 ºC during 24 hours and finally rise it up to 160 ºC for 30 hours. This aging treatment causes a dispersed location of the $MgZn_2$ precipitates [16], but with uniform and elongated grains, providing good corrosion resistance [5, 17].

iii) Retrogression and re-aging (rra), is applied in condition T6 to improve its corrosion resistance, keeping the high levels of resistance required for the structural applications of aircraft [18]. It consists of placing the sample at a temperature of 470 ° C for one hour, then cool it down to 120 ° C during 24 hours, then the temperature rises to 203 °C for 10 minutes and the thermal process is reduced to 120 °C for 24 hours [19]. The recoil temperature promotes the formation of more stable $MgZn_2$ precipitates [20,21]. The plates were joined at a 30º angle with welding without filler material with a current of 200 A.

X-ray diffraction of specimens were carried out in a Rigaku diffractometer, model Ultima IV, scintillation detector, Cu anode. Microscopic characterization of specimens was carried out by using a scanning electronic microscope (SEM) JEOL JSM-5900LV (15kV) attached with energy dispersive X-ray (EDX). For this, specimens were mounted in a polymeric resin, prepared by grinding on SiC metallographic paper from 240 to 1000-grit, polished with alumina (0.5 μm) followed by successively cleaning in ethanol and then distilled water using an ultrasonic bath for 15 min.

2.2. Corrosion tests

Once the treatments were done, the samples were polished with silicon carbide emery paper of different grains (500, 800, 1000, 1200, 1500 and 2000) in a Leco Spectrum System 1000 polishing machine, as well as with different particles size of alumina (1µm, 0.3 µm and 0.05µm). After polishing, an ultrasonic cleaning was done on the polished metal surface, exposing it during 15 minutes in ethanol. The samples were encapsulated with epoxy resin and a 80% Ni-20 Cr wire was welded as conductor. To evaluate the corrosion behavior of the different composites, normally aerated 3.5 % NaCl solution (pH= 8) was used with the aid of potentiodynamic polarization curves, electrochemical impedance spectroscopy (EIS) and linear polarization resistance measurements (LPR). For this, a three electrode cell was used, with a saturated calomel electrode (SCE) as reference a graphite rod as auxiliary electrode respectively. Before starting the tests, specimens were left during 20-30 minutes until the open circuit potential value was stable. Once this was attained, sweeping started for the polarization curves starting in a potential value of -600 mV at a scan rate of 1 mV/s, finishing in an anodic potential value of +1500 mV. Tafel extrapolation method was used to obtain corrosion current density values, I_{corr}. For the linear polarization resistance measurements (LPR), specimens were polarized from -10 to +10 mV around the free corrosion potential value, E_{corr}, at a scan rate of 1 mV/s every 60 minutes during 24 hours. Tests lasted 24 hours. Finally, electrochemical impedance spectroscopy (EIS) experiments were performed at the E_{corr} value by applying an AC signal of 10 mV peak-to-peak in the interval of frequencies of 0.1-100 kHz. A model PC4 300 Gamry potentiostat was used for this. Corroded surfaces of composites samples were established by scanning electronic microscope (SEM) JCM-6000 Plus.

3. RESULTS AND DISCUSSION

3.1 Materials characterization

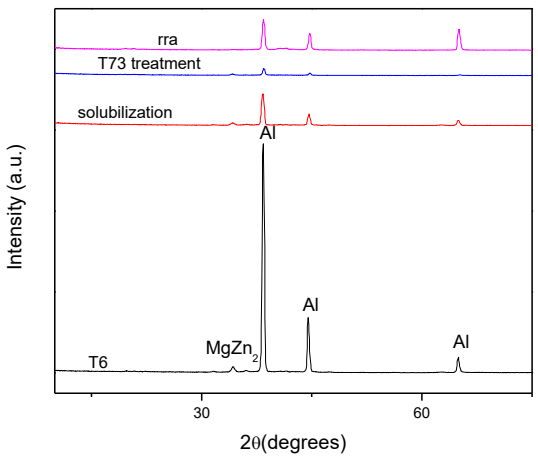

Figure 1. Effect of heat treatment on the X-ray diffraction patterns for 7075 aluminum alloy.

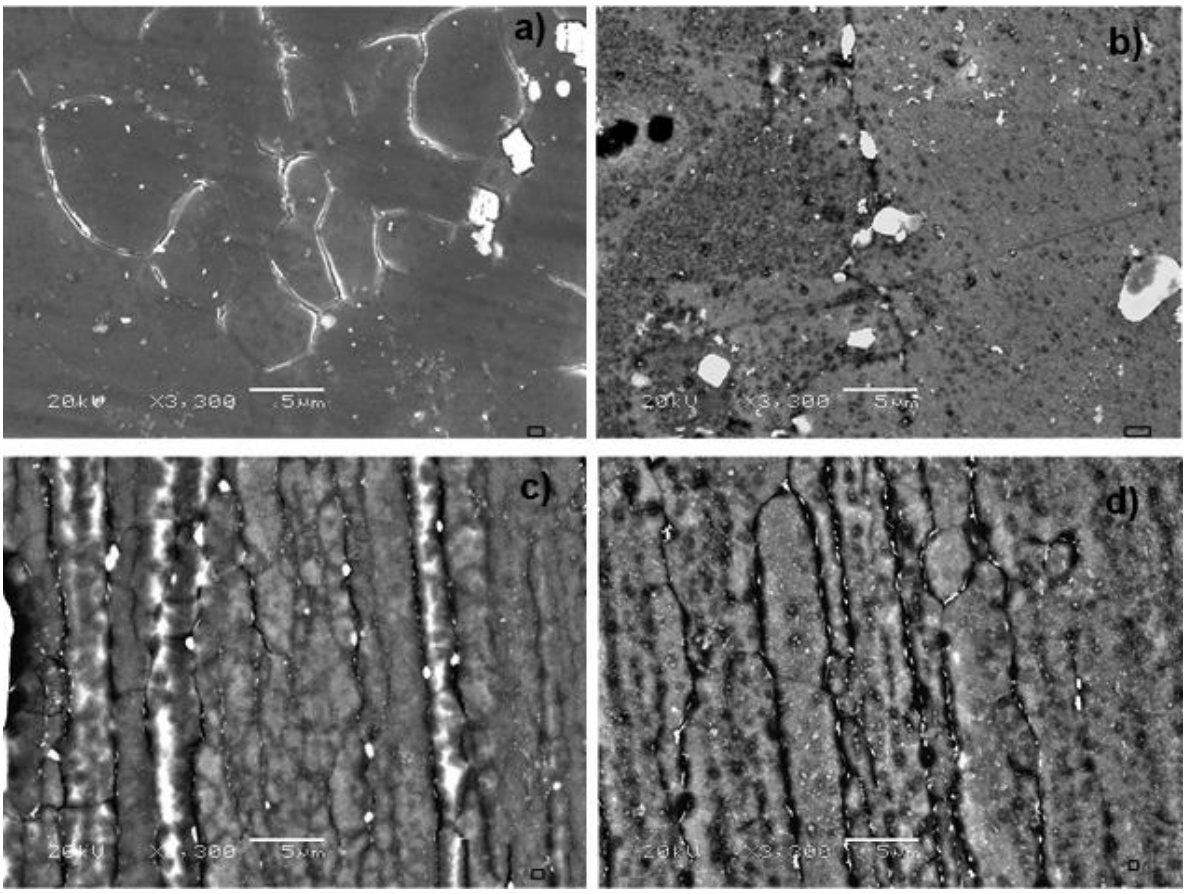

Figure 2. SEM micrographs of 7075 aluminum base alloy in the following heat treatments a) T6, b) solubilization, c) T73 and d) rra.

X-ray patterns for the specimens under different heat treatments are shown in Fig. 1. For the T6 treatment, the peaks that predominate are located in the angles 2θ = 38.48 (111), 44.66 (200) and 64.95 (220) related to α-Al (FCC). According to the quantitative analysis of the phases (RIR method) Al is in a proportion of 99.05% whereas the $MgZn_2$ phase is present in 0.9%. Secondary phases included weak reflection peaks of $MgZn_2$ precipitates that are located at angles 2θ = 41.17 with Miller index (201). According to the calculations made by the Halder - Wagner method, the crystal size is 287 ± 15 Å. For the solubilized specimen, according to the result obtained from the RIR method, an increase in the crystalline phase $MgZn_2$ is observed with a percentage of 4.02%, which is related to an increase in the intensity of 2θ = 41.17 degrees (201). The crystal size, according to the Halder-Wagner method, is reduced to a value of 230 ± 2 Å. For samples under T73 and rra heat treatments, the diffraction analysis shows the presence of peaks due to the crystalline phase $MgZn_2$ at 2θ = 40.61 and 41.15. The quantitative analysis shows an increase in the content of the $MgZn_2$ phase of 9.89% and 8.72% respectively. This is due to the exposure time of the sample in the aged and the high solubility of zinc and magnesium in the aluminum, which generates a high density of precipitates.

Microstructures obtained for the different heat treatments can be observed in Fig. 2. For specimen under the T6 heat treatment, microstructure consists of a transition η' phase which has big grains and fine precipitates (Fig. 2 a). For the solubilized specimen, Fig. 2 b, the formation of the η phase ($MgZn_2$)

and the dissolution of the η' (MgZn) phase can be observed. This is consistent with the x-ray patterns shown in Fig. 1 where an increase in the precipitates with respect to the T6 condition could be seen. Employed temperature for the T73 treatment allows an increase in the precipitates size, which are located mainly along the grain boundaries, where η phase ($MgZn_2$) is the main found phase, Fig. 2 c. Finally, for the rra treatment, Fig. 2 d, the presence of elongated grains can be observed, with an enlargement of the η phase ($MgZn_2$) along the grain boundaries with some of them finely dispersed within the grains.

3.2 Electrochemical behavior

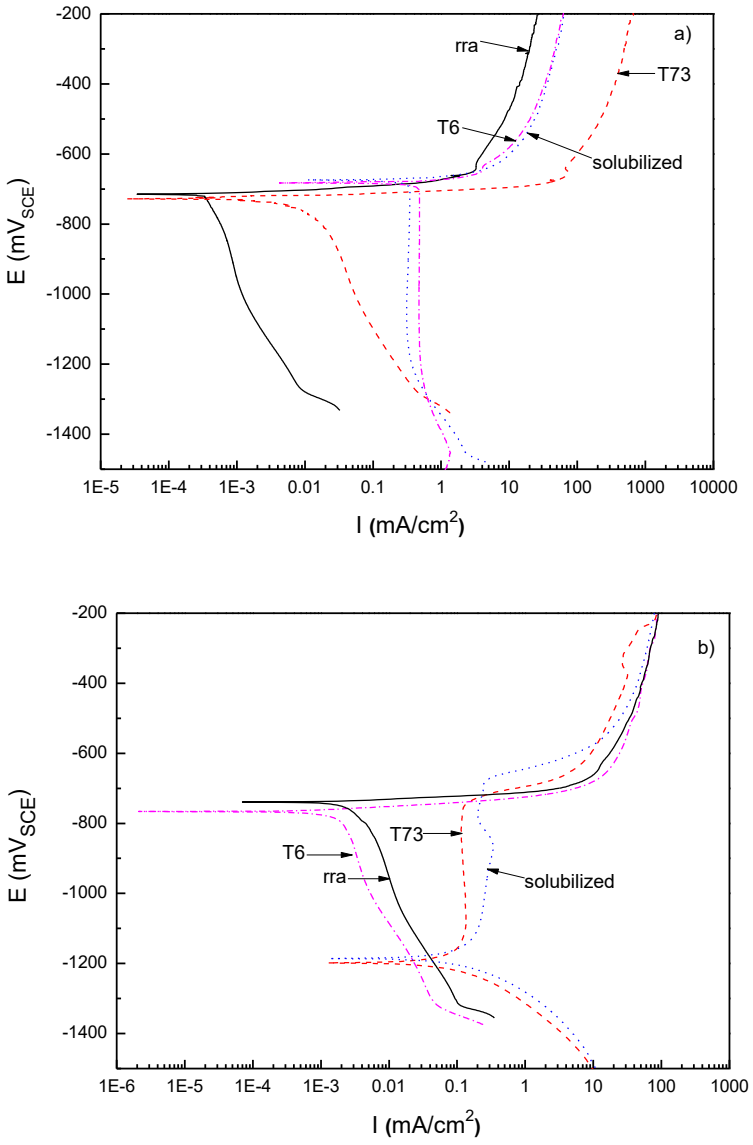

Figure 3. Effect of heat treatment on the polarization curves for 7075 aluminum alloy in the a) base metal and b) welded condition in 3.5 % NaCl solution.

The effect of heat treatment on the polarization curves for 7075-T6 aluminum alloy is given in Fig. 3. For the base metal, Fig. 3 a, curves displayed an active-passive behavior, and an E_{corr} value which

was only marginally affected by the heat treatment, see table 2, fluctuating between -680 and -730 mV. Curves displayed a very rapid increase in the anodic current density with the applied over potential from the E_{corr} value up to approximately -640 mV for all heat treatments, where the passive zone, due to the formation of an Al_2O_3 layer started regardless of the heat treatment [11].

Table 2. Electrochemical parameters obtained from polarization curves.

Heat treatment	Base metal		Welding	
	E_{corr} (mV)	I_{corr} (mA/cm^2)	E_{corr} (mV)	I_{corr} (mA/cm^2)
T6	-685	0.50	-770	2.0 x 10^{-3}
rra	-720	3.7 x 10^{-4}	-750	4.0 x 10^{-3}
T73	-730	1.0 x 10^{-2}	-1190	0.08
solubilization	-680	0.4	-1180	0.14

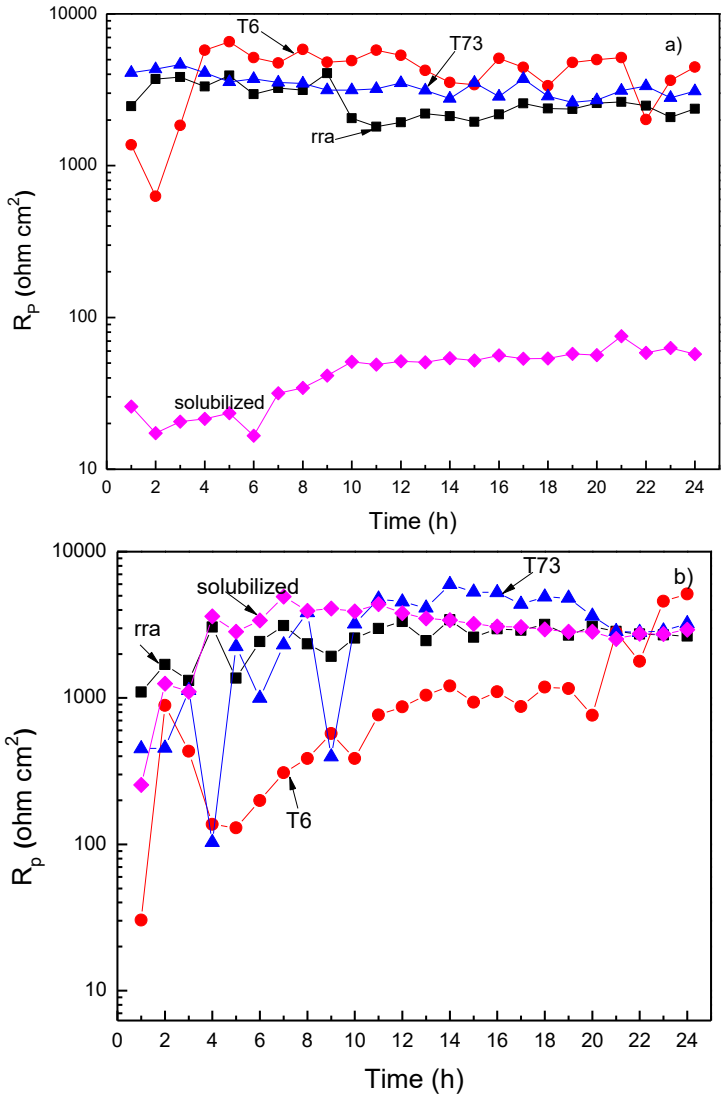

Figure 4. Effect of heat treatment on the Rp value for 7075 aluminum alloy in the a) base metal and b) welded condition in 3.5 % NaCl solution.

The highest corrosion current density value, I_{corr}, was for the T6 and solubilized conditions, with values very close to each other, between 0.4 and 0.5 mA/cm^2, whereas the rra and T73 treatments exhibited much lower I_{corr} values. 3.7 x 10^{-4} and 1.0 x 10^{-2} mA/cm^2 respectively. On the other hand, for the welding condition, Fig. 3 b, the behavior was very similar to the base metal for the T6 and rra treatments, exhibiting E_{corr} values around -760 mV and a very fast increase in the anodic current density value with the applied over potential up to a potential value close to -660 mV where the passive zone started. However, for the T73 and solubilization treatments, the E_{corr} value was shifted towards the active zone, reaching values fluctuating between -1180 and -1190 mV with I_{corr} values of 0.08 and 0.14 mA/cm^2, much higher than those found for the T6 and rra treatments, which exhibited I_{corr} values between 2.0 and 4.0 x 10^{-3} mA/cm^2 respectively. However, the passive current density values were much lower, nearly two orders of magnitude, for the formers, indicating a much more stable passive layer.

Since polarization curves are a kind of instant picture of the metal state which do not necessarily remains the same with as time elapses, the effect of heat treatment on the variation of the polarization resistance value with time, R_p, for both the base metal and welding are shown in Fig. 4. For the base metal, Fig. 4 a, the lowest R_p value, and, since I_{corr} and R_p are inversely proportional, the highest corrosion rate, was exhibited by the metal in the solubilized condition. The highest R_p value, around 8,000 ohm cm^2, and thus the lowest I_{corr} value, was for the metal under the T6 treatment, whereas that value for the T73 and rra treatments oscillated between 2,000 and 4, 000 ohm cm^2. It is worth it to note that, for the base metal, all the R_p values remained more or less constant through all the testing time, indicating that the formed Al_2O_3 layer was very stable under these conditions. For the welding condition, Fig. 4 b, the metal under the T6 condition exhibited the lowest R_p value, which started in a value close to 30 ohm cm^2 and it increased as time elapsed until it reached a value of 5, 000 ohm cm$^{2:}$ The R_p value for the metal under the rest of the heat treatments exhibited very similar values to each other, between 3,000 and 5,000 ohm cm^2.

The effect of the heat treatment on the Nyquist and Bode diagrams for the base metal and the welding conditions are given in Figs. 5 and 6 respectively. Nyquist diagrams, Figs. 5 a and 6 a, display a capacitive loop at high and intermediate frequency values followed by a straight-line at lower frequency values, typical of an Al alloy undergoing a localized type of attack such as pitting corrosion [22] due to localized galvanic attack of the more active matrix by the more noble MgZn and $MgZn_2$ phases. The high frequency semicircle is due to the film formed by the dissolution of the alloy whereas the straight line is related to the diffusional process occurring inside the pits. Bode diagrams, Fig. 5 b, shows that the impedance is maximum for the alloy in the rra and solubilized treatments for the base metal and welding respectively; on the other hand, this parameter reaches its lowest value in the solubilized condition for the base metal and in the T6 condition for the welding, Fig. 6 b. Thus, due to the microstructural changes induced during the welding procedure, we can see that under the same heat treatment can have different corrosion behavior. The plot of the log (impedance) versus the log (frequency) has two different slopes, and thus, the existence of two time constants, typical of an Al-alloy in a passive state [22]. Phase angle was maximum for the rra and T6 treatments for the base metal and welding respectively, and it shows the existence of two overlapped peaks, indicating the existence of two time constants; this peak is shifted towards lower frequencies for the other heat treatments, and it

decreased until it reached its lowest value for the alloy in the solubilized and rra conditions in the base metal and welding respectively.

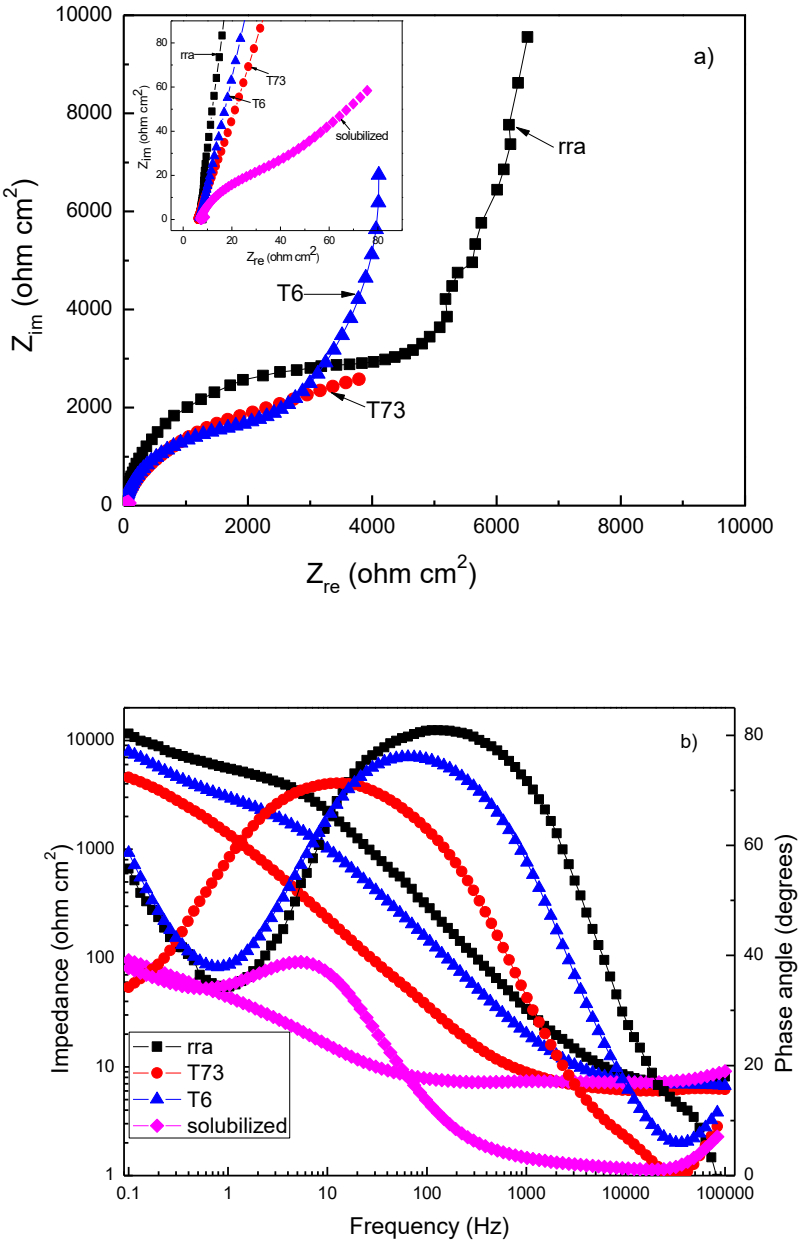

Figure 5. Effect of heat treatment on the a) Nyquist and b) Bode diagrams for 7075 aluminum base alloy in 3.5 % NaCl solution.

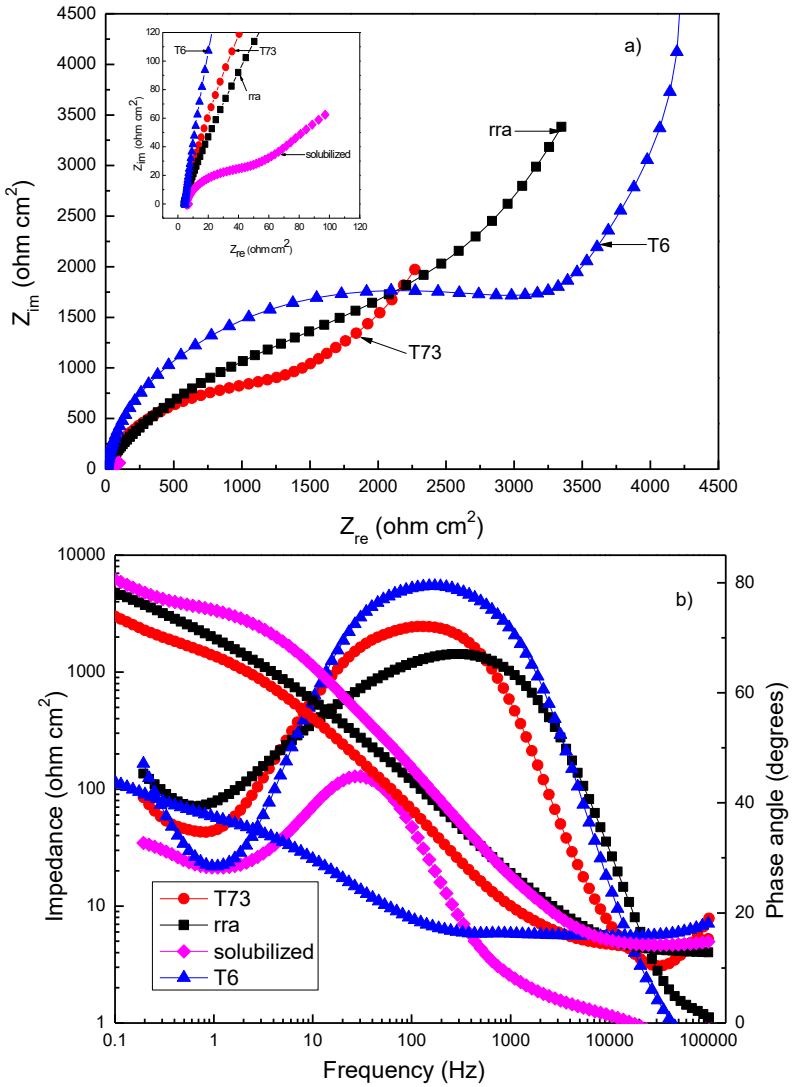

Figure 6. Effect of heat treatment on the a) Nyquist and b) Bode diagrams for welded 7075 aluminum in 3.5 % NaCl solution.

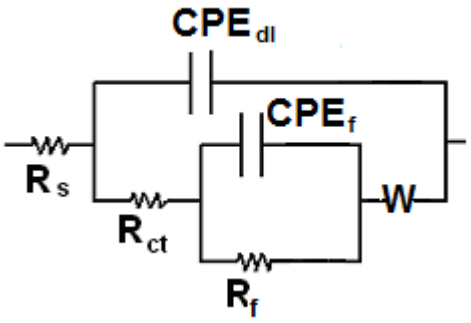

Figure 7. Electric circuit to simulate the EIS response of 7075 aluminum alloy under different heat treatments in 3.5 % NaCl solution.

The impedance behavior of the different composites can be described by equivalent circuits shown in Fig. 7. In these circuits, R_s corresponds to the solution resistance, CPE_{dl} and R_{ct} are the double electrochemical layer capacitive behavior and charge transfer resistance, CPE_f and R_f are the capacitive behavior of the corrosion products film and its resistance, whereas W is the Warburg diffusion element and R_w the diffusion layer resistance. Since the obtained semicircles are not perfect due to surface heterogeneities, we are not dealing with an ideal capacitor, and a constant phase element, CPE, was used to describe non-ideal capacitive behavior. We can use equation (1) to obtain the impedance of a CPE as follows:

$$Z_{CPE} = \frac{1}{Y_0(j\omega)^n} \quad (1)$$

where Y_0 is the magnitude of the CPE, j is $\sqrt{-1}$, ω is the angular frequency , and n is a parameter, between 0 and 1, and provides some surface parameters such as roughness [29].

Table 3. Parameters used to fit the EIS data for 7075 base aluminum alloy.

Heat treatment	R_{ct} (ohm cm^2)	n_{ct}	CPE_{dl} ($\mu Ss^n/cm^2$)	R_f (ohm cm^2)	n_f	CPE_f ($\mu Ss^n/cm^2$)	R_w (ohm cm^2)
rra	3.93×10^3	0.9	7.75×10^{-6}	6.7×10^3	0.9	5.5×10^{-6}	2.4×10^{-2}
solubilization	3.62×10^1	0.8	2.62×10^{-3}	1.6×10^2	0.8	4.3×10^{-4}	1.7×10^{-2}
T6	2.24×10^3	0.9	1.95×10^{-5}	3.0×10^3	0.9	6.1×10^{-5}	2.6×10^{-1}
T73	4.84×10^3	0.8	1.35×10^{-4}	1.8×10^3	0.8	6.6×10^{-4}	6.3×10^1

Table 4. Parameters used to fit the EIS data for 7075 welded aluminum alloy.

Heat treatment	R_{ct} (ohm cm^2)	n_{ct}	CPE_{dl} ($\mu Ss^n/cm^2$)	CPE_f ($\mu Ss^n/cm^2$)	R_f (ohm cm^2)	n	R_w (ohm cm^2)
rra	5.72×10^2	0.8	4.05×10^{-5}	6.6×10^{-5}	7.68×10^3	0.9	3.4×10^{-2}
solubilization	1.71×10^1	0.9	7.19×10^{-4}	5.4×10^{-4}	1.01×10^2	0.8	2.8×10^{-2}
T6	3.06×10^3	0.9	1.76×10^{-5}	3.4×10^{-6}	$2.15E \times 10^3$	0.9	3.3×10^{-1}
T73	8.68×10^2	0.9	5.67×10^{-5}	1.3×10^{-5}	2.72×10^3	0.8	5.3×10^1

Obtained parameters by using circuits shown in Fig. 7 are given in tables 3 and 4 for base metal and welding respectively. For both the base alloy and welding, the values for R_f are, in general terms, higher than those for R_{ct}, indicating that the corrosion resistance of these alloys is given mainly by the layer of corrosion products formed on top of them, nominally a layer which consists basically of a form of Al_2O_3 [11]. The diffusion resistance value, which, as stated above, refers to the diffusion inside the pits, is much lower than the R_f and R_{ct}, indicating that for this material, localized type of corrosion dominates over the uniform type of corrosion. However the R_{ct} value for the Al-base alloy is higher than that for the welding, as expected, since the corrosion resistance of the later was lower than the former. In addition to this, for both the base metal and welding, the R_w value for the rra and solubilized treatments was lower than that for the T6 and T73 treatments, indicating that the localized corrosion dominates over the uniform type of corrosion for the former whereas for the later uniform type of corrosion dominates

over the localized type of corrosion. To confirm this, the corroded surface of the different specimens were observed in the SEM (Fig. 8).

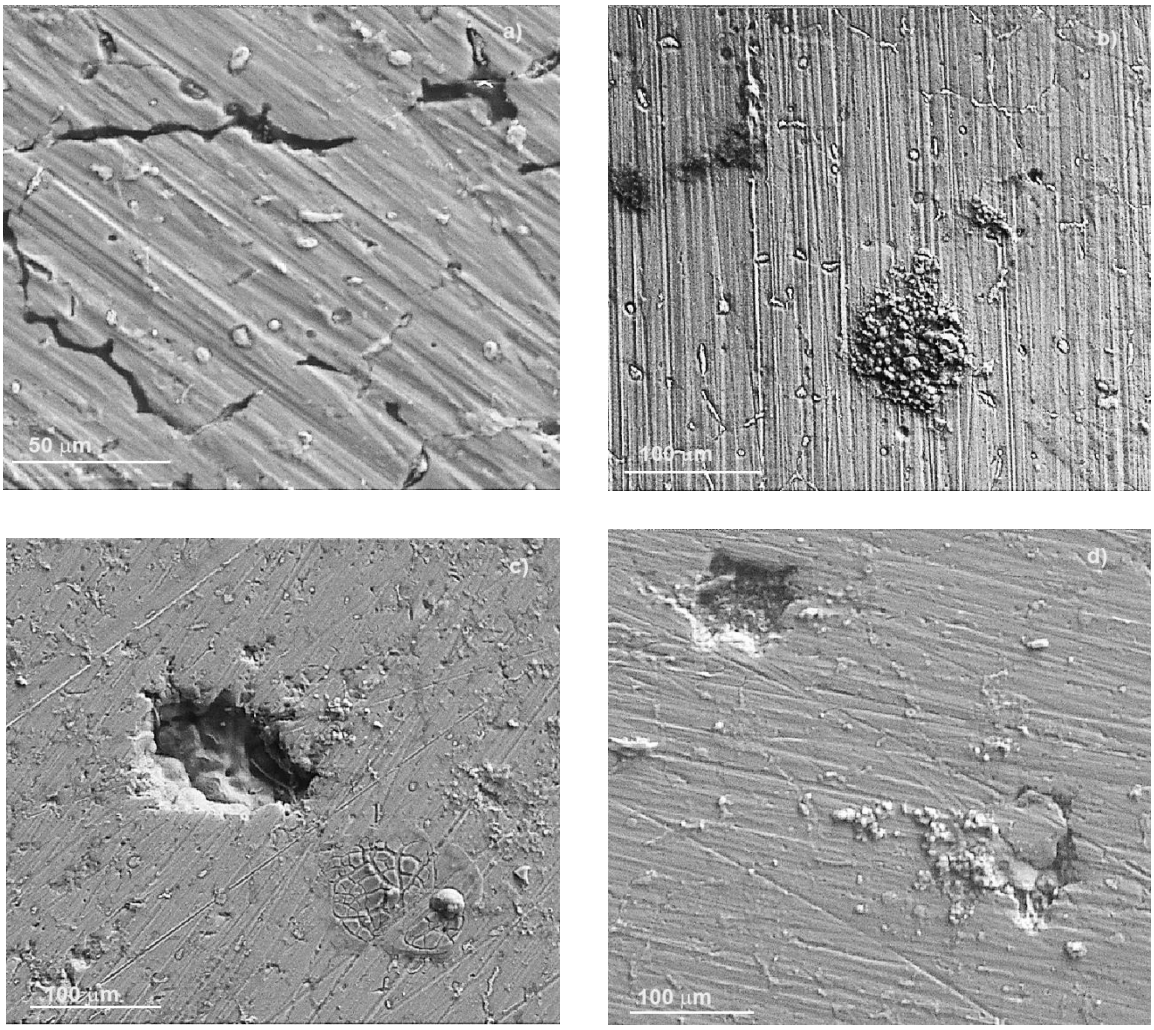

Figure 8. SEM micrographs of corroded 7075 aluminum base alloy in the following heat treatments a) T6, b) solubilization, c) rra and d) T73.

For the T6 condition, it is very evident, Fig. 8 a, that corrosion takes place around the $MgZn_2$ precipitates, leaving these precipitates uncorroded, and once the attack has penetrated deep enough, these precipitates are washed away, leaving voids in the places where the precipitates were located. Something similar is occurring for the solubilized specimen, Fig. 8 b, where it can be seen that corrosion takes place around the $MgZn_2$ precipitates which act as cathodes, whereas the surrounding matrix acts as active anode. This was not so evident for the specimens in the rra and T73 treatments, Figs. 8 c and d, where only the presence of localized type of corrosion can be observed in both specimens.

4. CONCLUSIONS

A study on the effect of heat treatment and welding condition on the corrosion behavior of 7075T6 Al alloy without material contribution has been investigated. Heat treatments included

solubilization at a temperature of 470 °C, retrogression and re-aging (rra), and T73. Main found phase included $MgZn_2$. Polarization curves showed the presence of a passive film regardless of the heat treatment in both the base metal and the welding although it was more stable for the solubilized and T73 treatments for the welding. LPR tests showed that the corrosion rates were very similar for the base metal and welding. However, for the base metal, the highest corrosion rate was exhibited for the solubilized condition, whereas for the welding it was for the T6 treatment. All specimens were highly susceptible to localized type of corrosion where the $MgZn_2$ phases acted as cathodes and the surrounding matrix acted as active anodes being dissolved away.

References

1. B. Prabhu, C. Suryanarayana, L. A. and R. Vaidyanathan, *Mater. Sci. Eng*. *A*, 425 (2006) 192.
2. J. Milligan, R. Vintila and M. Brochu*, Mater. Sci. Eng. A*, 508 (2009) 43.
3. N. Kang, P. Coddet, H. Liao, T. Baur and C. Coddet, *Appl. Surf. Sci*., 378 (2016) 142.
4. D. Yang, X. Li, D. He, Z. Nie and H. Huang, *Mater. Des.,* 34 (2012), 655.
5. N. Chawla and K. K. Chawla, Metal Matrix Composites, Springer Science and Business Media, Inc., (2006) NY., USA.
6. N. Alatorre, R. R. Ambriz, A. Amrouche, C. García and D. Jaramillo, *J. Mater. Process. Technol.*, *248* (2017) 207.
7. S. D. Thoppul and R. F. Gibson, *Mater. Charact.*, 60 (2009) 1342.
8. Q. Han, S. Viswanathan, *Metallurgical and Materials Transactions*, 34A (2003) 139.
9. H. T. Kim and S.W. Nam, *Scripta Mater.*, 34(1996) 1139.
10. A. D. Isadare, B. Aremo, M. O. Adeoye and O. J. Olawale, M. D. Shittu, *Mater. Res.*, 16(2013) 190.
11. M. Ö. Öteyaka and H. Ayrture, *Int. J. Electrochem. Sci.,* 10 (2015) 8549.
12. D. A. Necsulescu *UPB Sci. Bull*, 73 (2011) 223.
13. C. Yang, W. Gu, H. Zhang, R. Qiu, J. Hou and Y. Fu, *Int. J. Electrochem. Sci.,* 8 (2013) 9308.
14. K. Rajan, W. Wallace and J.C. Beddoes, *J. Mat. Sci*. 17(1982) 2817.
15. D. Zuluaga-Castrillón, J. Colorado-Marín, J. Gómez-Pérez, C. Suárez-Mercado, C.P. Serna-Giraldo and R. E. Aristizábal-Sierra, *Tecnol.*, 10 (2017) 23.
16. Y.S. Huang, T.S. Shih, J.H. Chou, *App. Surf. Sci*., 283 (2013) 249.
17. C.P. Ferrer, M.G. Koul, B.J. Connolly, A.L. Moran, *Corrosion*, 59(2003) 520.
18. R.T. Holt, R. Wallace, W. Wallace and D.L. Du Quesnay, *Mater. Charact.,* 35 (1995) 41.
19. J.F. Li, Z.W. Peng, C.X. Li, Z.Q. Jia, W.J. Chen and Z.Q. Zheng, (2008). *T. Nonferr. Met. Soc.,* 18 (2008) 755.
20. J.K. Park, *Mater. Sci. Eng.*, 103A (1988) 223.
21. F. Viana, A.M.P. Pinto, H.M.C. Santos and A. B. Lopes, (1999). *J. Mater. Process. Technology,* 92 (1999) 54.
22. R. Arraba, B. Mingo, A. Pardo, M. Mohedano, E. Matykina and I. Rodriguez, Corros. *Sci.,* 73 (2013) 342.

© 2019 The Authors. Published by ESG (www.electrochemsci.org). This article is an open access article distributed under the terms and conditions of the Creative Commons Attribution license (http://creativecommons.org/licenses/by/4.0/).